THE EUROPEAN
PHYSICAL JOURNAL C

QGP probes from a dynamical holographic model of AdS/QCD

S. Heshmatian[1,a] , **R. Morad**[2,3,b]

[1] Department of Engineering Sciences and Physics, Buein Zahra Technical University, Buein Zahra, Qazvin, Iran
[2] UNESCO UNISA ITL/NRF Africa Chair in Nanosciences/Nanotechnology, College of Graduate Studies, University of South Africa (UNISA), Pretoria, South Africa
[3] Nanosciences African Network, Materials Research Department, iThemba LABS, National Research Foundation, Cape Town, South Africa

Abstract   In this paper, we employ the gauge/gravity duality to study some features of the quark–gluon plasma. For this purpose, we implement a holographic QCD model constructed from an Einstein–Maxwell-dilaton gravity at finite temperature and finite chemical potential. The model captures both the confinement and deconfinement phases of QCD and we use it to study the effect of temperature and chemical potential on a heavy quark moving through the plasma. We calculate the drag force, Langevin diffusion coefficients and also the jet quenching parameter, and our results align with other holographic QCD models and the experimental data.

Contents

1 Introduction

Quark–gluon plasma (QGP) produced at the Relativistic Heavy Ion Collider (RHIC) and the Large Hadron Collider (LHC) is a strongly coupled plasma whose dynamics is dominated by non-perturbative effects [1,2]. Since the perturbative quantum chromodynamics (QCD) is applicable only in the weak coupling regime, the lattice QCD techniques could be hired for understanding the static equilibrium thermodynamics of such matter. Alternatively, the "AdS/CFT correspondence" [3–7] provides a non-perturbative tool to examine the dynamical quantities of the strongly coupled QGP. The "AdS/CFT correspondence" indicates a duality between the $\mathcal{N} = 4\, SU(N_c)$ super-Yang–Mills theory and type IIB string theory on $AdS_5 \times S^5$, which is a powerful tool to study the strongly coupled gauge theory in the large N_c limit and large 't Hooft coupling. The original duality maps an asymptotically AdS space to a conformal gauge theory at zero temperature. On the other hand, due to the fact that the physical quantities of the quark–gluon plasma are temperature dependent, many attempts were made to extend the original duality to holographic models describing the QGP at finite temperature using top-down [8–10] or bottom-up models [11–39].

One of the interesting features of QCD is the confinement-deconfinement crossover where the QCD coupling constant becomes very large. This phenomenon leads to a strong suppression of quarkonium near the crossover temperature, as the confined phase of QCD is at a lower temperature and density compared to the deconfined phase [40–42]. Lattice QCD calculations demonstrate that the entropy of the quark–antiquark pair develops a peak around the crossover area [43,44] which indicates the strong interaction between the quark–antiquark pair in this region. The quark–antiquark entropy in both phases and the confinement-deconfinement crossover have both been thoroughly studied utilizing the AdS/CFT correspondence and generalized dual holographic models [45–50].

Among holographic models of QCD, the model constructed from a black hole solution using the Einstein–Maxwell-dilaton gravity is beneficial as it incorporates the temperature dependency of the entropy of the quark–antiquark pair in both confined and deconfined phases [51,52]. On the other hand, this holographic model includes

[a] e-mail: heshmatian@bzte.ac.ir (corresponding author)

[b] e-mail: rmorad@tlabs.ac.za

Springer

chemical potential as the QCD equation of state and phase diagram depends on the chemical potential. On the gravity side, increasing temperature leads to a phase transition from thermal AdS to a black hole using a specific choice of an arbitrary function $A(z)$. In the boundary theory, these are dual to phase transitions from confined to deconfined phases. The results of this model for the quark–antiquark entropy are in good agreement with those from Lattice QCD and therefore, this holographic model could be a capable model to study the QCD feature in confined and deconfined phases. The gravity solution was then extended with a magnetic field to analyzed the quark–antiquark free energy and entropy from holographic point of view [53–55].

Jets of quarks propagating through the medium are the most interesting objects produced in QGP and their interaction with the medium is one of the challenging problems in new physics. The transport coefficient, also known as the jet quenching parameter, is one of the most interesting experimental observables associated with quark energy loss in the hot medium observed at RHIC and LHC [56–63]. It is defined as the average squared transverse momentum transferred from a traversing parton to the medium, per unit mean free path [64]. The parton energy loss through the medium can also be investigated using the drag force experienced by heavy quarks moving in the medium. Due to the strong nature of the interaction, holographic models of QCD are utilized as powerful tools to investigate the dynamics of this phenomena and characterize properties of jets and QGP medium as well as their interactions which leads to the quark energy loss. Also, heavy quarks moving in QGP undergo a Brownian-like motion which could be studied by the Langevin diffusion coefficients [65,66].

According to the AdS/CFT correspondence, a heavy quark is illustrated as a fundamental string attached to a flavor brane. The string endpoint could be considered as a quark in the boundary theory and the string itself can be considered as a gluonic cloud surrounding the quark. The drag force of a quark moving in the medium can be measured from the corresponding momentum flowing of an open trailing string to the bulk [67–85]. The quantum fluctuations of this trailing string are also dual to the momentum broadening of a heavy quark moving in the QGP and can be computed along the quark direction of the motion as well as the transverse plane. The stochastic Brownian motion is associated with the correlators of the string fluctuations and can be expressed in terms of the Langevin coefficients [83–99]. According to this duality, the jet quenching parameter is related to the thermal expectation value of the light-like Wilson loop operator created from the trajectory of two string endpoints, and many attempts were made to compute this parameter in the context of the AdS/CFT correspondence [100–127]. The holographic energy loss of a quark moving in a strongly coupled QGP has been studied in [121] for a strongly coupled

anisotropic $\mathcal{N} = 4$ super Yang–Mills plasma and also, in [128] using another version of the Einstein–Maxwell-dilaton model where the anisotropy is introduced at one spatial direction in metric [129].

In this paper, we study the QGP aspects such as the drag force, Langevin coefficients, and the jet quenching parameter for a heavy quark moving through the plasma using the gauge/gravity duality. For this purpose, we implement the dynamical holographic QCD model of Ref. [52] as the dual boundary theory involves temperature in both confined and deconfined phases as well as the chemical potential and has a qualitative agreement with Lattice results for the quark–antiquark entropy in both confined and deconfined phases, therefore it would be an appropriate model to examine the QGP features.

This paper is organized as follows: In Sect. 2 we briefly review the holographic QCD model constructed from the Eintein–Maxwell-dilaton gravity introduced in [52]. In Sect. 3 we discuss the drag force on heavy quark moving in the dynamical holographic model of QCD. In Sect. 4, the Langevin coefficients are calculated. In Sect. 5, the jet quenching parameter is studied, and in Sect. 6, a summary and conclusion are presented.

2 Einstein–Maxwell-dilaton gravity

In this section, we review the Einstein–Maxwell-dilaton gravity (EMD) model at finite and zero temperature [51,52] which is described by the following action in 5 dimensions,

$$S_{EM} = -\frac{1}{16\pi G_5} \int d^5x \sqrt{-g}$$
$$\times \left[R - \frac{f(\phi)}{4} F_{MN} F^{MN} - \frac{1}{2} \partial_M \phi \partial^M \phi - V(\phi) \right]. \quad (1)$$

where G_5 is the Newton constant, $V(\phi)$ is the potential of the dilaton field and $f(\phi)$ is the gauge kinetic function representing the coupling between the dilaton and the gauge field A_M.

By assuming the following ansatz for the metric, gauge field, and dilaton field,

$$ds^2 = \frac{L^2 e^{2A(z)}}{z^2} \left(-g(z)dt^2 + dx_1^2 + dx_2^2 + dx_3^2 + \frac{dz^2}{g(z)} \right),$$
$$A_M = A_t(z), \quad \phi = \phi(z), \quad (2)$$

where L is the AdS length scale and fields are assumed to be functions of extra radial coordinate z, one can solve the equations of motion analytically in terms of $A(z)$ and $f(z)$ [11,12]

$$g(z) = 1 - \frac{\int_0^z dx \, x^3 e^{-3A(x)} \int_{x_c}^x dx_1 \, \frac{x_1 e^{-A(x_1)}}{f(x_1)}}{\int_0^{z_h} dx \, x^3 e^{-3A(x)} \int_{x_c}^x dx_1 \, \frac{x_1 e^{-A(x_1)}}{f(x_1)}},$$

$$\phi'(z) = \sqrt{6(A'^2 - A'' - 2A'/z)},$$

$$A_t(z) = \sqrt{\frac{-1}{\int_0^{z_h} dx\, x^3 e^{-3A(x)} \int_{x_c}^x dx_1\, \frac{x_1 e^{-A(x_1)}}{f(x_1)}}}$$

$$\times \int_{z_h}^z dx\, \frac{x e^{-A(x)}}{f(x)},$$

$$V(z) = -\frac{3z^2 g e^{-2A}}{L^2} \left[A'' + A'\left(3A' - \frac{6}{z} + \frac{3g'}{2g}\right) \right.$$
$$\left. -\frac{1}{z}\left(-\frac{4}{z} + \frac{3g'}{2g}\right) + \frac{g''}{6g} \right]. \tag{3}$$

The spacetime asymptotic boundary is located at $z = 0$ where $g(z)$ goes to 1, and $z = z_h$ is the position of the horizon with the boundary condition of $g(z_h) = 0$. It is shown that by considering the simple form of $f(z) = e^{cz^2 - A(z)}$, one can reproduce the linear Regge trajectory of the discrete spectrum of the mesons. The value of $c = 1.16$ GeV^2 is fixed by matching the holographic meson mass spectrum to the lowest-lying heavy meson states [11].

The gravity solution corresponds to a black hole with horizon located at z_h, is then given by

$$g(z) = 1 - \frac{1}{\int_0^{z_h} dx\, x^3 e^{-3A(x)}}$$
$$\times \left[\int_0^z dx\, x^3 e^{-3A(x)} + \frac{2c\mu^2}{(1 - e^{-cz_h^2})^2} \det \mathcal{G} \right],$$

$$\phi'(z) = \sqrt{6(A'^2 - A'' - 2A'/z)},$$

$$A_t(z) = \mu \frac{e^{-cz^2} - e^{-cz_h^2}}{1 - e^{-cz_h^2}},$$

$$V(z) = -\frac{3z^2 g e^{-2A}}{L^2} \left[A'' + A'\left(3A' - \frac{6}{z} + \frac{3g'}{2g}\right) \right.$$
$$\left. -\frac{1}{z}\left(-\frac{4}{z} + \frac{3g'}{2g}\right) + \frac{g''}{6g} \right], \tag{4}$$

where μ is the chemical potential and

$$\det \mathcal{G} = \begin{vmatrix} \int_0^{z_h} dx\, x^3 e^{-3A(x)} & \int_0^{z_h} dx\, x^3 e^{-3A(x) - cx^2} \\ \int_{z_h}^z dx\, x^3 e^{-3A(x)} & \int_{z_h}^z dx\, x^3 e^{-3A(x) - cx^2} \end{vmatrix}.$$

The Hawking temperature and entropy of this solution are

$$T = \frac{z_h^3 e^{-3A(z_h)}}{4\pi \int_0^{z_h} dx\, x^3 e^{-3A(x)}} \left[1 + \frac{2c\mu^2 \left(e^{-cz_h^2} \int_0^{z_h} dx\, x^3 e^{-3A(x)} - \int_0^{z_h} dx\, x^3 e^{-3A(x)} e^{-cx^2}\right)}{(1 - e^{-cz_h^2})^2} \right]$$

$$S_{BH} = \frac{L^3 e^{3A(z_h)}}{4G_5 z_h^3}. \tag{5}$$

There is another solution for the Einstein–Maxwell-dilaton equations which corresponds to a thermal-AdS space. This solution is obtained by taking the $z_h \to \infty$ limit of the

solution (4) which results in $g(z) = 1$. The chemical potential goes to zero in this limit and therefore, the thermal gas solution has zero chemical potential. This thermal solution is asymptotically AdS. Nevertheless, it can have a non-trivial structure in the bulk due to the scale factor $A(z)$.

It should be highlighted that, traditionally, one would construct a gravitational background by fixing $V(\phi)$ and solve the Einstein equations. Instead, for the model summarized here, the background is constructed by fixing $A(z)$ which leads to an implicit dependency on T and μ for the dilaton potential. Consequently, the thermodynamic laws are slightly violated. This is a known issue for this construction method, however, it has been verified that the dependency of dilaton potential on these parameters is generally minor. For more detail please refer to [53].

For the holographic model to describe the confinement-deconfinement phases in the boundary theory, the following form of $A(z)$ is being considered

$$A(z) = A_2(z) = -\bar{a}z^2, \tag{6}$$

which vanishes at the boundary. The value of $\bar{a} = c/8 \simeq 0.145$ is determined such that the Hawking/Page phase transition occurs at $T \simeq 270 MeV$ at zero chemical potential. With this choice of $A(z)$, the thermodynamic properties of the solution are shown in Figs. 1 and 2.

In Fig. 1a, the temperature of the solution is plotted in terms of z_h. At each temperature, for small values of μ, there are two solutions: large black hole (small z_h) and small black hole (large z_h). The small black hole solution is thermodynamically unstable. Also the black hole solution only exist above a minimum temperature, T_{min} indicating there is a first order phase transition from black hole to thermal-gas phase. Although, this transition happens at some critical temperature T_c above the T_{min}. In Fig. 1b, the ratio of critical temperature to the minimum temperature is plotted for different values of μ. This ratio is always larger than one and enhanced by increasing the chemical potential. Increasing the value of chemical potential in Fig. 1a, the branch with negative slope (the small black hole solution) becomes smaller and completely vanishes at some critical chemical potential $\mu = \mu_c = 0.673$. At $\mu > \mu_c$, we have a single black hole solution which remains stable at all temperatures.
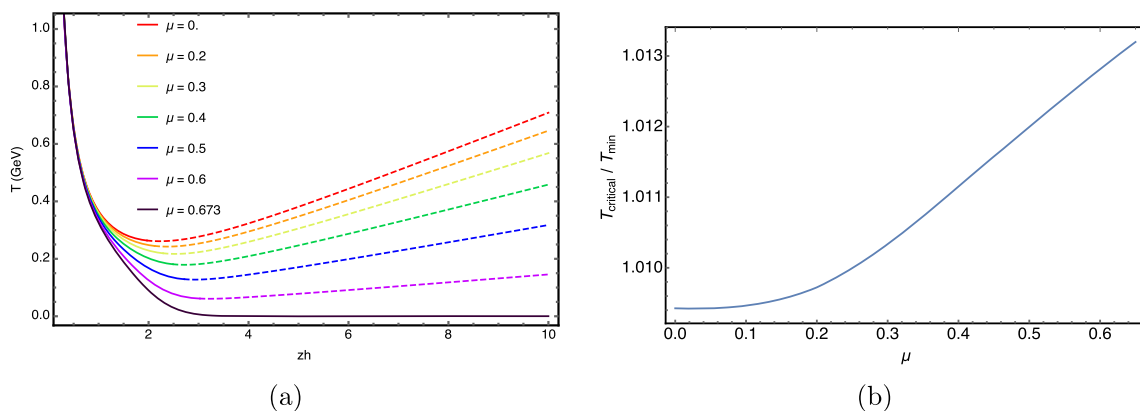
Fig. 1 **a** The temperature of the solution versus z_h for different values of μ. **b** The ratio of critical temperature to the minimum temperature for different values of μ. Stable solutions are represented by solid lines while dashed lines characterize the unstable solutions

In Fig. 2a, the normalized entropy of the system is plotted in terms of temperature. By increasing temperature, this ratio reaches the value of one. In Fig. 2b, the free energy of the solution is plotted in terms of the temperature. The free energy is normalized such that the free energy of thermal-AdS is zero. Therefore, changing the sign of free energy means a first-order phase transition from AdS black hole to thermal-AdS as the temperature decreases which takes place at $T = T_c$. This is the famous Hawking-Page phase transition. In [52], this Hawking-Page phase transition on the gravity side is used to determine the confinement/deconfinement phase transition on the dual boundary side. They used the phase for which the free energy of the probe quark–antiquark pair varies linearly with respect to their separation length, as confinement. Here, we explore this confinement/deconfinement phase transition using the external probes on the gravity side.

In order to study the holographic probes we are interested in, it is more convenient to use the string frame metric which can be obtained using the following standard transformations,

$$(g_s)_{MN} = e^{\sqrt{\frac{2}{3}}\phi} g_{MN}, ds_s^2 = \frac{L^2 e^{2A_s(z)}}{z^2}$$
$$\times \left(-g(z)dt^2 + \frac{dz^2}{g(z)} + dx_1^2 + dx_3^2 + dx_3^2\right), \quad (7)$$

where $A_s(z) = A(z) + \sqrt{\frac{1}{6}}\phi(z)$. The open string tension T_s in units of the AdS length scale L^2 is considered to be $T_s L^2 \simeq 0.1$ [52], which is obtained by comparing the numerical results with the lattice QCD estimate of the string tension, i.e. $\sigma_s \approx 1/(2.34)^2 \, \text{GeV}^2$ [55].

3 Drag force

In this section, we consider a heavy quark moves with a constant velocity in one of the spatial directions denoted by x. Therefore, the embedding function of a heavy quark in the static gauge $\tau = t, \sigma = z$ is $X = \{t, x(t,z), z\}$. The action of a fundamental string is given by the Nambu- Goto action as,

$$S = -\frac{1}{2\pi\alpha'} \int d\sigma \, d\tau \, \sqrt{-\gamma}$$
$$= -\frac{1}{2\pi\alpha'} \int d\sigma$$
$$\times d\tau \sqrt{-G_{tt}G_{zz} - G_{tt}G_{xx}x'^2 - G_{xx}G_{zz}\dot{x}^2}, \quad (8)$$

where dot and prime are derivatives with respect to τ and σ and G represent the components of the background metric. In order to study the dynamics of string, we use the metric of Eq. (7). In the static gauge, the corresponding Lagrangian density takes the following form,

$$\mathcal{L} = -\frac{1}{2\pi\alpha'} \frac{e^{2A_s(z)}}{z^2} \sqrt{1 - \frac{\dot{x}^2}{g(z)} + g(z)x'(z)^2}. \quad (9)$$

Then the equation of motion for x is,

$$\partial_t \left(\frac{\dot{x}}{\sqrt{-\gamma'}}\right) - \frac{z^2 g(z)}{e^{2A_s(z)}} \partial_z \left(\frac{e^{2A_s(z)} g(z)x'}{z^2\sqrt{-\gamma'}}\right) = 0. \quad (10)$$

The static string stretching from the boundary to the horizon, $x(t, z) = Constant$ is a trivial solution of this equation. For a string whose endpoint at the boundary moves with a constant velocity v, the following ansatz is chosen,
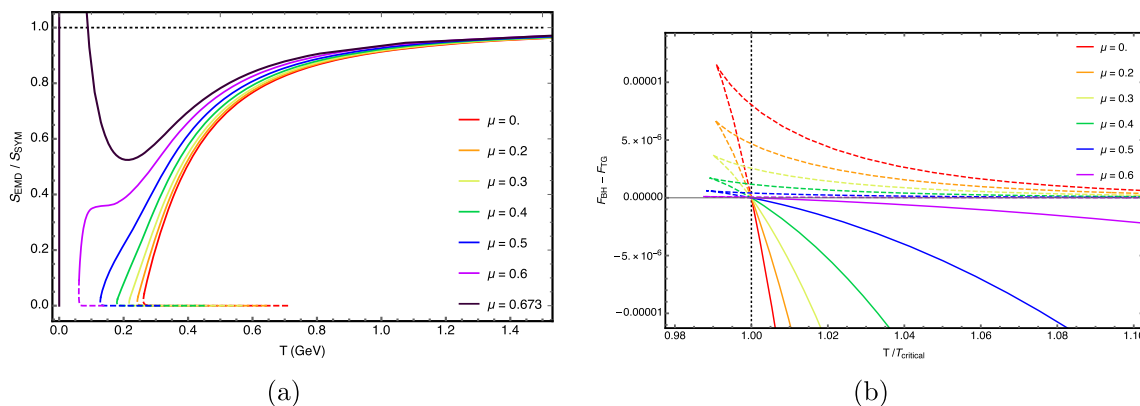
(a)

(b)

Fig. 2 **a** The ratio of black hole entropy to the AdS Schwarzschild black hole entropy versus temperature for different values of μ. **b** The free energy versus temperature for different values of chemical potential between zero (red) and $\mu = \mu_c$ (purple). For each value of μ, there is a phase transition between the AdS-BH and thermal gas solution.

Here, $\mu_c = 0.673\, GeV$ is the critical value for μ for which there is no phase transition and the large black hole solution exists from zero temperature to high temperature. Solid (Dashed) lines show the stable (unstable) solutions

$$X = \{t, vt + \xi(z), z\}, \tag{11}$$

which leads to the following equation of motion,

$$\frac{e^{2A_s(z)}g(z)\xi'(z)}{\sqrt{-\gamma}z^2} = const \equiv \pi_x, \tag{12}$$

where π_x is the worldsheet conserved quantity. One can obtain the equation for ξ as follows,

$$\xi'(z) = \pm \frac{\pi_x}{g(z)}\sqrt{\frac{g(z) - v^2}{\frac{e^{4A_s(z)}g(z)}{z^4} - \pi_x^2}}. \tag{13}$$

Requiring the real values for the function under the square root fixes the constant of the equation of motion as,

$$g(z_s) - v^2 = 0,$$
$$\frac{e^{4A_s(z_s)}g(z_s)}{z_s^4} - \pi_x^2 = 0 \implies \pi_x = \frac{e^{2A_s(z_s)}v}{z_s^2}. \tag{14}$$

Finally, substituting the Eq. (14) into the Eq. (13), one can solve the string solution,

$$\xi'(z) = -\frac{e^{2A_s(z_s)}v}{z_s^2}\frac{1}{g(z)}\sqrt{\frac{g(z) - g(z_s)}{\frac{e^{4A_s(z)}g(z)}{z^4} - \frac{e^{4A_s(z_s)}g(z_s)}{z_s^4}}}. \tag{15}$$

The canonical momentum densities associated to the string are,

$$\begin{pmatrix} \pi_t^0 \\ \pi_x^0 \end{pmatrix} = \frac{T_0 L^4}{\sqrt{-\gamma}}\frac{e^{4A_s(z)}}{z^4 g(z)}\begin{pmatrix} -g(z)\left(g(z)\xi'(z)^2 + 1\right) \\ v \end{pmatrix}, \tag{16}$$

$$\begin{pmatrix} \pi_t^1 \\ \pi_x^1 \end{pmatrix} = \frac{T_0 L^4}{\sqrt{-\gamma}}\frac{e^{4A_s(z)}}{z^4}\begin{pmatrix} -v\, g(z)\, \xi'(z) \\ g(z)\, \xi'(z) \end{pmatrix}. \tag{17}$$

Integrating the π_t^0 and π_x^0 along the string gives us the total energy and the total momentum in the direction of motion of

the string, respectively. While, π_t^1 and π_x^1 are the energy and momentum flow down along the string. It is straightforward to show that π_x^1 is exactly the constant of the equations of motions, π_x in Eq. (14). Also, just similar to the case of $\mathcal{N} = 4$ SYM plasma, $\pi_t^1 = -v\,\pi_x^1$. It means that if we pull the quark with the constant velocity, the fraction of energy flow at a given point along the string, π_t^1 is constant. This is the energy dissipating into the surrounding medium by the quark. Therefore, the drag force is obtained as,

$$F_{drag} = -\pi_x^1 = -\frac{1}{2\pi\alpha'}\frac{e^{2A_s(z_s)}v}{z_s^2}. \tag{18}$$

The drag force of the AdS Schwarzschild black hole background can be obtained analytically as [78,79],

$$F_{drag}^{SYM} = -\frac{\pi\,T^2\,\sqrt{\lambda}}{2}\frac{v}{\sqrt{1 - v^2}}, \tag{19}$$

while in this background, we first need to solve the Eq. (14) numerically to obtain the z_s, and then calculate the drag force using the Eq. (18).

In Fig. 3, the ratio of drag force to its conformal value is plotted in terms of temperature for two different quark velocities and different values of μ from zero to the critical value of 0.673. The solid curves represent the drag force ratio of the deconfined phase starting from the critical temperature T_c while the non-physical dashed curves correspond to the confined phase drag ratio. As mentioned in Sect. 2, a first-order phase transition from thermal AdS to black hole phase occurs by decreasing z_h, and for each chemical potential value, the critical temperature is the temperature in which the free energy sign changes. Therefore, there exist two solutions at each temperature, one for the thermal AdS solution and the other for the AdS Black hole solution. The drag ratio develops a peak around the critical temperature only for the high veloc-

ity $v = 0.99$. The peak moves towards higher temperatures for smaller values of chemical potential and higher quark velocities, as shown in red and orange curves inside Fig. 3a. For the deconfined phase, the drag force ratio increases by increasing the chemical potential value and decreasing the quark velocity. The same behavior in temperature and chemical potential has been reported in the holographic QCD model of [87] for the Einstein–Maxwell-scalar gravity system (also in [101] the same behavior on baryon chemical potential has been shown). From this figure, one could also find that at high temperatures, the curves of all chemical potential values converge and the drag force would be less than the value of $\mathcal{N} = 4\, SYM$ theory due to the smaller 't Hooft coupling of the holographic QCD model.[1] At lower temperatures, the drag force ratio is more sensitive to the chemical potential value, and the drag force of the holographic model is larger than the drag force of the $\mathcal{N} = 4 SYM$ theory for larger μ values. For lower quark velocities, the drag force ratio is less sensitive to the chemical potential (Fig. 3b).

The world-sheet coordinates can be reparametrized as,

$$\tau = t + K(z),$$
$$x = v\,t + v\,K(z) + \xi(z) . \tag{20}$$

Since, the dynamic of the string is independent from $K(z)$, one can choose the following ansatz,

$$K'(z) = -\frac{G_{xx}\, v}{G_{tt} + G_{xx}\, v^2}\, \xi'(z) . \tag{21}$$

By substituting the background metric components and using Eqs. (14), and (15), the induced metric simplifies as,

$$h_{\alpha,\beta} = \frac{L^2\, e^{2A_s(z)}}{z^2}$$
$$\times \begin{pmatrix} -(g(z) - v^2) & 0 \\ 0 & \dfrac{z_s^4\, e^{4A_s(z)}}{e^{4A_s(z)}\, g(z)\, z_s^4 - e^{4A_s(z_s)}\, g(z_s)\, z^4} \end{pmatrix} \tag{22}$$

which can be considered as the metric of a two-dimensional world-sheet black hole with the horizon radius of z_s. The local speed of light at the worldsheet horizon corresponds to the speed of a quark at the boundary. The associated Hawking temperature of the worldsheet is calculated numerically and its ratio to its conformal value is plotted in Fig. 4 for two different quark velocities. Similar to the drag force, the behavior of this ratio at lower temperatures, near the critical temperature, is very dependent on the chemical potential and quark velocity, such that for μ close to μ_c the worldsheet temperature in this background can be larger than its conformal value. However, at large temperatures, this ratio tends to one independent of the μ and quark velocity values. Similar

to the drag force ratio plot of Fig. 3, for each chemical potential value, the solid curve starts from its critical temperature and the solid and dashed curves correspond to the deconfined and confined phases respectively.

4 Langevin equation

Heavy quarks moving at a constant velocity in the plasma experience a Brownian motion which can be described by the effective equation of motion [78]

$$\frac{dp}{dt} = -\eta_D\, p + \xi(t), \tag{23}$$

where η_D is the drag coefficient, p is the relativistic expression of the momentum of the quark, and ξ is a random force, expressing the interaction of the medium with the heavy quark. This random force causes the momentum broadening of the quark which can be extracted by analyzing small fluctuations in the path of the Wilson line. This is dual to perturbing the location of the classical string endpoint on the boundary which yields fluctuations on the string world sheet dragging behind the quark. Therefore, we consider the quadratic fluctuations around the classical trailing string solution obtained in the previous section. In the static gauge, $\tau = t$, and $\sigma = z$, we generalise the embedding function of the string as

$$x_L(t, z) = v\,t + \xi(z) + \delta\,x(t, z) \quad , \quad x_T = \delta\,x_T(t, z), \tag{24}$$

where L and T denote to the parallel and transverse to the direction of motion. Now, we rewrite the Nambu-Goto action Eq. (8) and expand it to second order in terms of fluctuations around the string solution, Eq. (15)

$$S = -\frac{1}{2\pi\alpha'} \int dz\, dt\, \sqrt{-\gamma}\, \frac{\gamma^{\alpha\beta}}{2}$$
$$\times \left[N(z)\, \partial_\alpha \delta x_L\, \partial_\beta \delta x_L + G_{xx}\, \partial_\alpha \delta x_T\, \partial_\beta \delta x_T \right], \tag{25}$$

where

$$\gamma = \frac{L^4 z_s^4}{z^4}\, \frac{e^{8A_s(z)}(g(z) - v^2)}{e^{4A_s(z)} g(z) z_s^4 - e^{4A_s(z_s)} g(z_s) z^4}, \tag{26}$$

and

$$N(z) = \frac{L^2}{e^{2As(z)} z^2}\, \frac{e^{4A_s(z)} g(z) z_s^4 - e^{4A_s(z_s)} g(z_s) z^4}{z_s^4(g(z) - v^2)} . \tag{27}$$

The above action can be rewritten in terms of the world-sheet coordinate Eq. (20) and ansatz Eq. (21) which diagonalized the induced metric, Eq. (22)

$$S = -\frac{1}{2\pi\alpha'} \int dz\, dt\, \frac{H^{\alpha\beta}}{2}$$
$$\times \left[N(z)\, \partial_\alpha \delta x_L\, \partial_\beta \delta x_L + G_{TT}\, \partial_\alpha \delta x_T\, \partial_\beta \delta x_T \right], \tag{28}$$

---

[1] In this paper, we have considered $T_s L^2 = 0.1$ [52] which corresponds to a small 't Hooft coupling for the holographic QCD model compared to the $\mathcal{N} = 4 SYM$ coupling that is considered to be 6π.
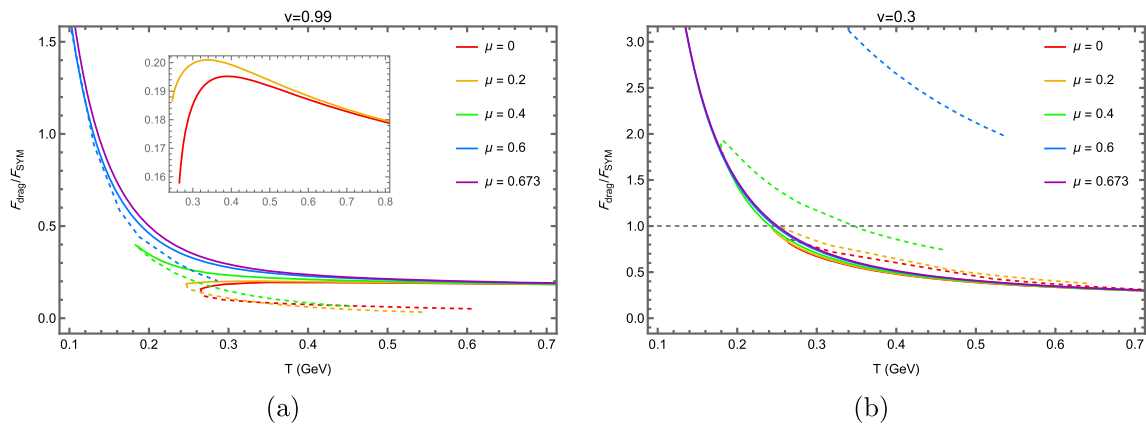
Fig. 3 The ratio of drag force in the holographic QCD model to its conformal value in terms of temperature for $\mu = 0, 0.2, 0.4, 0.6$ and 0.673 (red, orange, green, blue and violet respectively). The solid curves correspond to the deconfined phase and the dashed curves represent the data of the confined phase. **a** The velocity of quark is $v = 0.99$. **b** The velocity of quark is $v = 0.3$
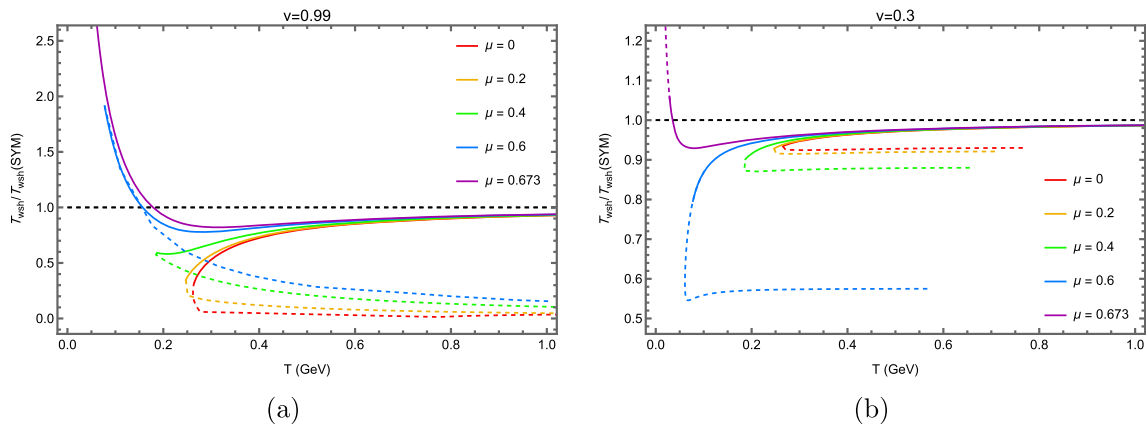

Fig. 4 The ratio of the worldsheet temperature of the holographic QCD model to its conformal value in terms of temperature for $\mu = 0, 0.2, 0.4, 0.6$ and 0.673 (red, orange, green, blue and violet respectively). The solid curves correspond to the deconfined phase and the dashed curves represent the ratio in the confined phase. **a** The velocity of quark is $v = 0.99$. **b** The velocity of quark is $v = 0.3$

where $H^{\alpha\beta}$ is defined in terms of inverse of the diagonalized induced metric Eq. (22) as

$$H^{\alpha\beta} = \sqrt{h}\,h^{\alpha\beta}, \tag{29}$$

One can read the transport coefficient directly from the above action according to the membrane paradigm [94]. The quadratic effective action for a massless scalar field ϕ has the form of

$$S = -\frac{1}{2}\int dz\,dt\,\sqrt{-g}\,q(z)\,g^{MN}\partial_M\phi\,\partial_N\phi. \tag{30}$$

The momentum broadening coefficients can be read directly from the above action as

$$\kappa = \lim_{\omega \to 0}\left(-\frac{2T_{wsh}}{\omega}\text{Im}\hat{G}_R(\omega)\right) = 2\,T_{wsh}\,q(z), \tag{31}$$

where $\text{Im}\hat{G}_R$ is the imaginary part of retarded correlation function at the world-sheet horizon. By comparing the

action 28 with Eq. (30) and implying the relation 31, the Langevin coefficients can be read as [7,95,96]

$$\kappa_T = \frac{1}{\pi\alpha'}\,T_{wsh}\,G_{xx}|_{z \to z_s}$$

$$\kappa_L = \frac{1}{\pi\alpha'}\,T_{wsh}\,N(z)|_{z \to z_s} \tag{32}$$

The final results for the ratio of the longitudinal to transverse transport coefficients in this model is

$$\frac{\kappa_L}{\kappa_T} = 1 + \frac{4g(z_s)\,(z_s\,A_s'(z_s) - 1)}{z_s\,g'(z_s)}, \tag{33}$$

where the L' Hospital's rule were employed since our functions are continuous and z_s is calculated using Eq. (14).

In Fig. 5, we have plotted the transverse and longitudinal transport coefficients versus temperature for two different quark velocities. In these plots, the black solid curves represent the κ_T and κ_L of the $\mathcal{N} = 4\,SYM$ theory, and the

dashed lines represent the data of the confined phase of the holographic model. From the deconfined curves, we find that increasing the temperature and chemical potential, increases the transport coefficients and for high quark velocity, the dependency on μ is more relevant. Also, one could observe that at lower temperatures (available for higher chemical potential values) the transverse and longitudinal transport coefficients are larger than the $\mathcal{N} = 4\,SYM$ while for smaller μ values, they are smaller than $\mathcal{N} = 4\,SYM$. Our numerical results for the transport coefficients obey the expected inequality in isotropic backgrounds $\kappa_L > \kappa_T$ [96].

The ratios of $\kappa_L/\kappa_{L(SYM)}$ and $\kappa_T/\kappa_{T(SYM)}$ in terms of the temperature for two quark velocities are shown in Fig. 6. At lower temperatures, the dependency on μ is more evident while at high temperatures, all the curves converge to a single value smaller than one. The data of each μ, exhibit a peak around the critical temperature that moves towards higher temperatures for smaller values of chemical potential (except for the small μ curves of Fig. 6b in which no peaks exist). From these plots, one could find that the transport coefficients increase by increasing the chemical potential similar to the transport coefficients in a medium with baryon density [101].

5 Jet quenching parameter

In this section, we study the light quark energy loss by calculating the jet quenching parameter. For this purpose, we follow the method of [100] to compute this parameter in the holographic QCD model of [51,52] reviewed in Sect. 2.

Starting from the string frame metric of Eq. (7) and using the light-cone coordinates $x^\pm = (x_1 \pm t)/\sqrt{2}$, the bulk metric takes the following form,

$$ds^2 = \frac{L^2\,e^{2A_s(z)}}{z^2}\left(dx_2{}^2 + dx_3{}^2 + \frac{1}{2}\left(1 - g(z)\right) \right.$$
$$\times \left(dx^{+2} + dx^{-2} \right)$$
$$\left. + \left(1 + g(z)\right) dx^+ dx^- + \frac{dz^2}{g(z)} \right). \tag{34}$$

To calculate the jet quenching parameter, the thermal expectation value of a closed rectangular Wilson loop is being used as [100],

$$\langle W^A(\mathcal{C}) \rangle \approx \exp\left[-\frac{1}{4\sqrt{2}} \hat{q}\, L^- L^2 \right], \tag{35}$$

where L^- is the distance (conjugate to partons with relativistic velocities) and L is the transverse distance (conjugate to the transverse momentum of the radiated gluons). This equation is valid for $L^- \gg L$. On the other hand, Thermal expectation value of the Wilson loop $\langle W^F(\mathcal{C}) \rangle$ is obtained

by using the extremal surface action as [45–47,103,104]

$$\langle W^F(\mathcal{C}) \rangle = \exp\left[-S_I(\mathcal{C}) \right], \tag{36}$$

where S_I is the normalized action of a hanging string from Wilson loop $\mathcal{C}$ joining two light-like lines. to the bulk (after subtracting the self energy of the $q\bar{q}$ pair from the Nambu-Goto action of the string worldsheet). In the large N_c limit, one can use the relation $\mathrm{Tr}_{(Adj.)} = \mathrm{Tr}^2{}_{(Fund.)}$ and compare the Eqs. (35) and (36) to obtain,

$$\hat{q} = \frac{8\sqrt{2}S_I}{L^- L^2}. \tag{37}$$

By the string parametrization $x^\mu(\tau, \sigma)$, the Nambu-Goto action of the string is written as,

$$S_{NG} = \frac{1}{2\pi\alpha'} \int d\sigma\, d\tau\, \sqrt{-\det \gamma_{\alpha\beta}}, \tag{38}$$

where $\gamma_{\alpha\beta}$ is the induced metric on the string worldsheet and the worldsheet coordinates $\sigma^\alpha = (\tau, \sigma)$ are set to be (x^-, x_2). The contour length along x_2-direction is defined by L and the length along τ-direction by L^-. The boundary conditions are $\phi(\pm\frac{L}{2}) = 0$ and $x_3(\sigma)$ and $x^+(\sigma)$ coordinates are constant. Then the action of Eq. (38) reads,

$$S_{NG} = \frac{L^-}{\sqrt{2}\pi\alpha'} \int_0^{\frac{L}{2}} d\sigma\, \frac{e^{2A_s(z)}}{z^2} \sqrt{\frac{1 - g(z)}{2}\left(1 + \frac{z'^2}{g(z)}\right)} \tag{39}$$

where prime denotes the derivative with respect to x_2. Since the Lagrangian density is time independent, the Hamiltonian of the system is constant,

$$\mathcal{L} - z' \frac{\partial \mathcal{L}}{\partial z'} = \frac{\Pi_z}{\sqrt{2}}. \tag{40}$$

From the above equation, one can obtain z' as,

$$z' = \sqrt{g(z)\left(\frac{e^{4A_s(z)}(1 - g(z))}{\Pi_z{}^2 z^4} - 1\right)}. \tag{41}$$

Integrating Eq. (41) leads to,

$$\frac{L}{2} = a_0 \Pi_z + \mathcal{O}(\Pi_z{}^3), \tag{42}$$

where,

$$a_0 = \int_{z_h}^0 dz \frac{z^2 e^{-2A_s(z)}}{\sqrt{g(z)\left(1 - g(z)\right)}}. \tag{43}$$

Here, we have considered that for small length L, the constant Π_z is small and its higher order terms are negligible. Substituting Eq. (41) into Eq. (39) yields,

$$S_{NG} = \frac{L^-}{\pi\alpha'} \int_{z_H}^0 dz \frac{e^{4A_s(z)}(1 - g(z))}{z^2\sqrt{2g(z)(e^{4A_s(z)}(1 - g(z)) + \Pi_z^2 z^4)}}, \tag{44}$$
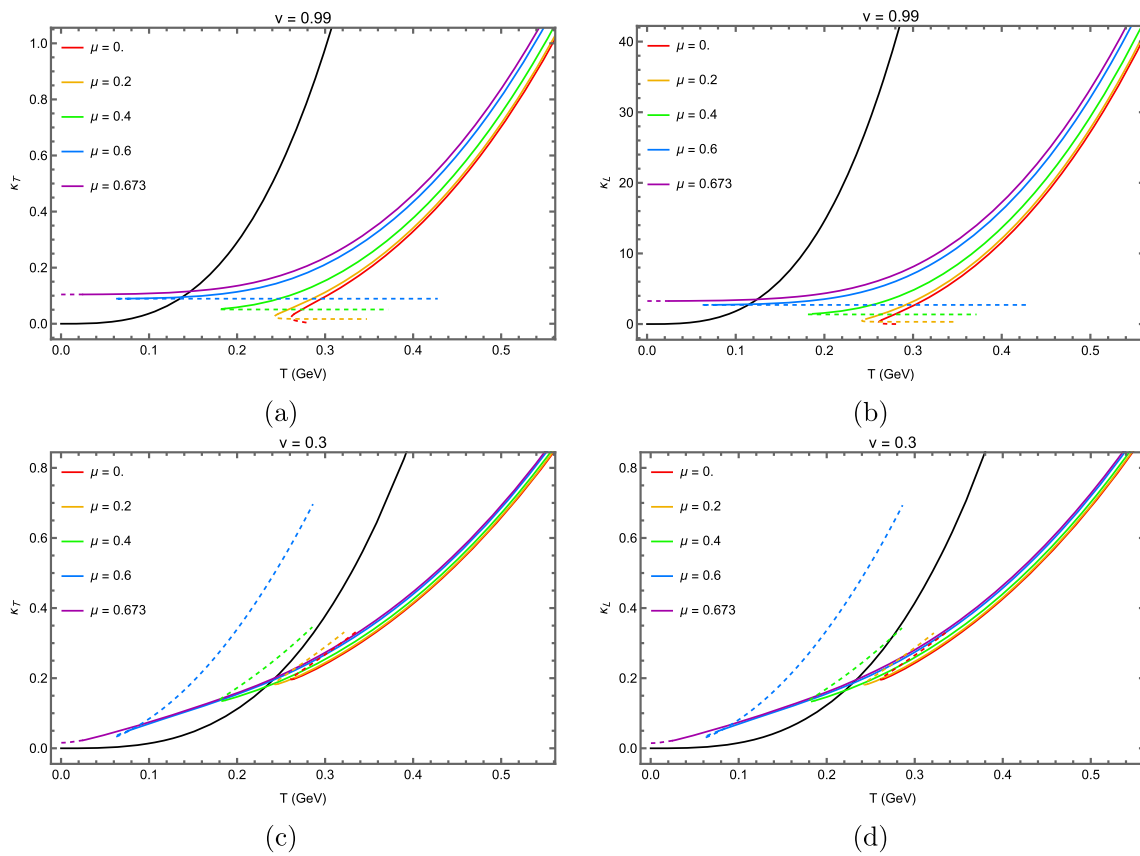
Fig. 5 The longitudinal and transverse transport coefficients in the holographic model in terms of the temperature for $\mu = 0, 0.2, 0.4, 0.6$ and 0.673 (red, orange, green, blue and violet respectively). **a** κ_T for $v = 0.99$, **b** κ_L for $v = 0.99$, **c** κ_T for $v = 0.3$ and **d** κ_L for $v = 0.3$

where we have used $z' = \frac{\partial z}{\partial \sigma}$. Expanding this equation for small Π_z, leads to,

$$S_{NG} = \frac{L^-}{\pi \alpha'} \int_{z_H}^{0} dz \frac{e^{2A_s(z)}}{z^2} \sqrt{\frac{1 - g(z)}{2g(z)}}$$
$$\times \left(1 + \frac{e^{-4A_s(z)} \Pi_z^2 z^4}{2(1 - g(z))} + ...\right), \quad (45)$$

This action diverges and one should subtract the self energy of two disconnected strings whose worldsheets are located at $x_2 = \pm \frac{L}{2}$ and extended from boundary to horizon as,

$$S_0 = \frac{L^-}{2\pi \alpha'} \int_{z_H}^{0} dz \sqrt{g_{--} g_{zz}}$$
$$= \frac{L^-}{2\pi \alpha'} \int_{z_H}^{0} dz \frac{e^{2A_s(z)}}{z^2} \sqrt{\frac{1 - g(z)}{2g(z)}}. \quad (46)$$

The normalized action is therefore,

$$S_I = S_{NG} - 2S_0 \equiv \frac{L^- \Pi_z^2 a_0}{2\sqrt{2\pi} \alpha'}. \quad (47)$$

Inserting Eq. (47) into Eq. (37) leads to the following expression for the jet quenching parameter of holographic model,

$$\hat{q} = \frac{1}{\pi \alpha' a_0}, \quad (48)$$

where we have used Eq. (42) for Π_z and a_0 is the numerical integral defined in Eq. (43). For $\mathcal{N} = 4$ supersymmetric Yang–Mills theory in the large N_c and large λ limits, Eq. (48) leads to the following analytical equation [100],

$$\hat{q}_{SYM} = \frac{\pi^{3/2} \Gamma(\frac{3}{4})}{\Gamma(\frac{5}{4})} \sqrt{\lambda} \, T^3, \quad (49)$$

In order to obtain the jet quenching parameter for the holographic QCD model of [52], we have solved the equation of 48 numerically for different values of temperature (z_h) and chemical potential. The resulting curves are plotted in Fig. 7. In this figure, the numerical values of the jet quenching parameter are shown for the holographic QCD model (red, orange, green, blue, and purple curves with $\mu = 0, 0.2, 0.4, 0.6$ and μ_c respectively). Solid curves correspond to the deconfined phase of the holographic model and dashed curves represent the confined phase data. For each chemical potential value, the solid curve starts from the criti-
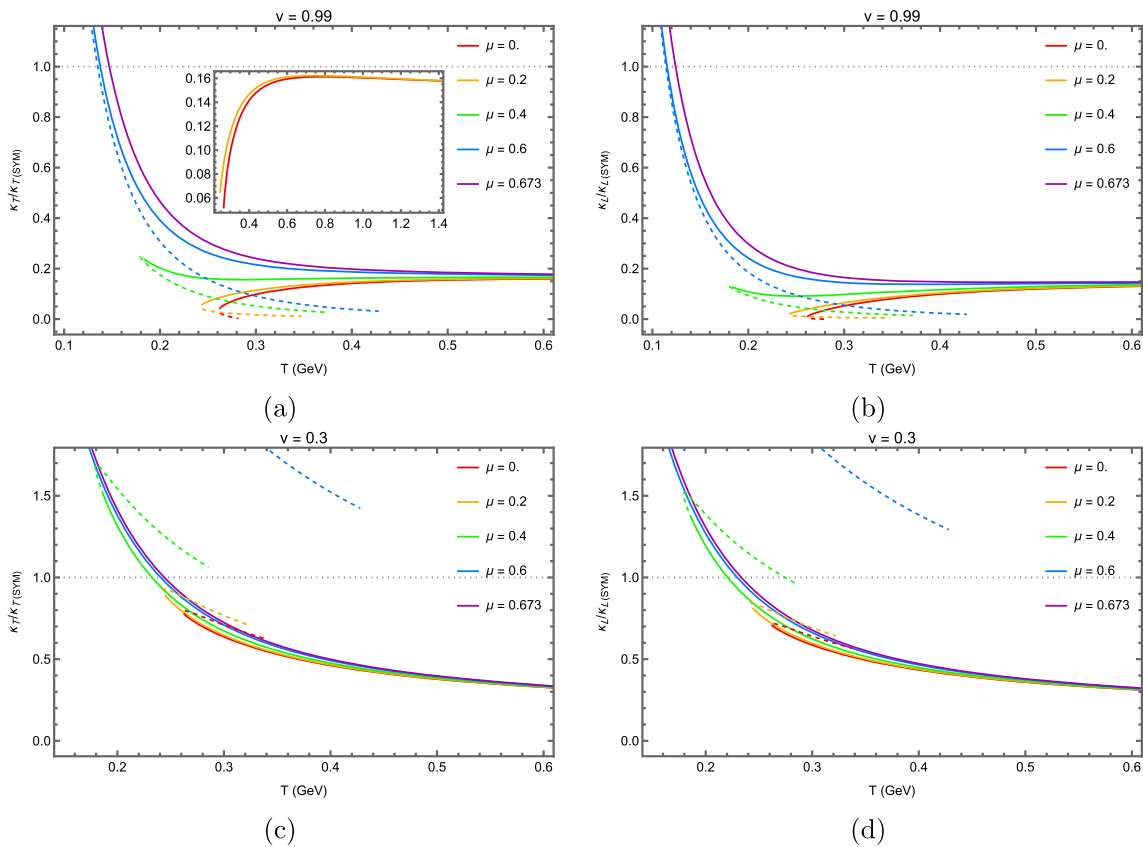
(a)

(b)

(c)

(d)

Fig. 6 The ratio of the longitudinal to transverse transport coefficients in the holographic model in terms of the temperature for $\mu = 0, 0.2, 0.4, 0.6$ and 0.673 (red, orange, green, blue and violet respectively). **a** The transverse ratio for $v = 0.99$, **b** the longitudinal for $v = 0.99$, **c** the transverse ratio for $v = 0.3$ and **d** the longitudinal ratio for $v = 0.3$

cal temperature T_c, at which the confinement/deconfinement phase transition occurs. In this figure, the solid black curve displays the $\hat{q}_{SYM}$ and the black circles with error bars are the absolute values of $\hat{q}$ for a 10 GeV quark jet in the most central Au-Au collisions at RHIC with the highest temperature $T = 0.37 GeV$ and Pb-Pb collisions at LHC with the highest temperature $T = 0.47 GeV$ [63].[2] From this figure, one can observe that increasing the chemical potential and temperature leads to an increase of the jet quenching parameter. At lower temperatures associated with larger values of chemical potential, $\hat{q} > \hat{q}_{SYM}$ and at higher temperatures, $\hat{q} < \hat{q}_{SYM}$. Experimental values of the jet quenching parameter, are closer to the higher chemical potential curves.

The ratio of the jet quenching parameter in the holographic QCD model to the $\hat{q}_{SYM}$ is plotted in Fig. 8a in terms of temperature for $\mu = 0, 0.2, 0.4, 0.6$ and μ_c. From this figure, one could observe that at higher temperatures, the jet quenching curves converge to a value lower than the corresponding
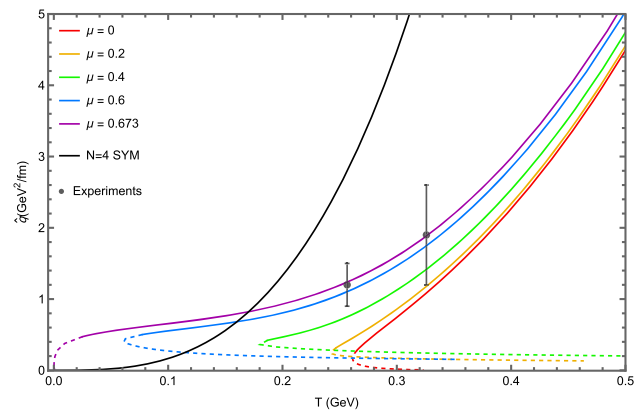
Fig. 7 Jet quenching parameter versus temperature for the holographic model with different chemical potentials. The black curve is $\hat{q}_{SYM}$ and the circles indicate the experimental values from RHIC and LHC. The dashed curves represent the jet quenching parameter for the confined phase and the colored solid curves stand for the deconfined phase of the holographic model

---

[2] In this plot, these two temperatures are rescaled as $T \approx T_{SYM} = 3^{-1/3}T_{QCD}$ since for the holographic QCD theories, the number of degrees of freedom is more than those of 3 favor QCD [63].

value of the $\mathcal{N} = 4$ SYM theory similar to the curves of the drag force and Langevine coefficients in Figs. 3 and 6. However, at lower temperatures, the jet quenching parameter of
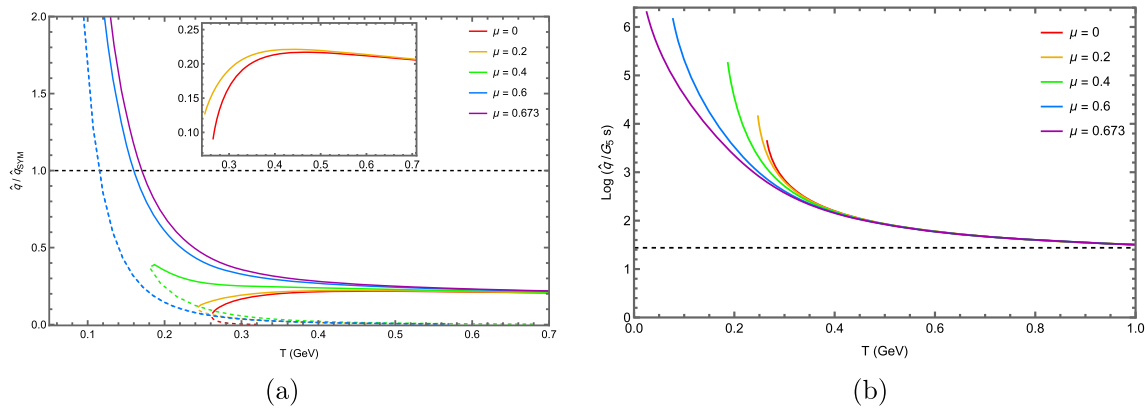
Fig. 8 **a** $\hat{q}/\hat{q}_{SYM}$ and **b** $Log(\hat{q}/G_5 s)$ versus temperature for the holographic QCD model. Red, orange, green, blue and violet curves correspond to $\mu = 0, 0.2, 0.4, 0.6$ and 0.673 respectively)

the holographic QCD model is larger than the $\hat{q}_{SYM}$. Similar to Figs. 3a and 5a for a high-velocity heavy quark, increasing the chemical potential value, increases this ratio, and the $\hat{q}/\hat{q}_{SYM}$ plot indicates a smooth confinement/deconfinement phase transition that results in a peak around the critical temperature for $\mu < \mu_c$ (for smaller μ's, the peak shifts to higher temperatures). The same behavior has been observed for $\hat{q}/T^3$ in the dynamical holographic QCD model of [102] suggesting the rapid changing in the system degrees of freedom during the phase transition [101, 102].

Finally, the logarithmic plot of the jet quenching parameter over the entropy density is plotted in terms of the temperature in Fig. 8b (in units of G_5) for different values of chemical potential. The dashed line represents the logarithmic value of $\hat{q}/G_5 s$ for the $\mathcal{N} = 4$ SYM theory and each curve has a sharp rise with a finite peak at the crossover temperature. The peak increases by increasing the chemical potential and is higher than the $\hat{q}/s$ curves of [102]. It is worth mentioning that, despite the different concept and calculation methods, the jet quenching parameter of a light quark has the same behavior as the transverse transport coefficient of a high-velocity heavy quark (and consequently, to the Langevin jet quenching parameter $\hat{q}_T = 2\kappa_T/v$).

6 Conclusion

In this paper, we studied the drag force and the Langevin diffusion coefficients for a heavy quark and also, the jet quenching parameter for a light quark moving through the QGP. For this purpose, we have implemented the holographic QCD model of [52] as a realistic framework for the QCD confinement/deconfinement phase transition with thermodynamic properties consistent with QCD and lattice data.

Our results demonstrate a nontrivial behavior on temperature and chemical potential, especially near the phase transition temperature. For a high-velocity heavy quark, the drag force and the transverse transport coefficient ratios increase

by increasing the chemical potential. For each chemical potential value, these ratios develop a peak around the critical temperature that shifts to higher temperatures for higher quark velocities and smaller values of chemical potential. The longitudinal transport coefficients exhibit the same behavior except for the lower values of the chemical potential where no peaks exist. For a low-velocity quark, the drag force and transport coefficients ratios, monotonically decrease by increasing temperature and are less sensitive to the chemical potential values.

Also, we have calculated the jet quenching parameter for a light-like trajectory in terms of temperature for different values of chemical potential. This parameter, increases by increasing the chemical potential and temperature. Our results are in good agreement with the experimental data from RHIC and LHC. The ratios of $\hat{q}/\hat{q}_{SYM}$ are more than one at lower temperatures (accessible to the higher values of chemical potential). Similar to the drag force and transport coefficients, the curves develop peaks around the crossover temperature and at high T's, converge to a single value less than one due to the small 't Hooft coupling of the holographic QCD model we have implemented here. The jet quenching parameter of a light quark and the transverse transport coefficient of a high-velocity heavy quark, display the same qualitative behavior despite the differences. In the end, the ratio of $\hat{q}/G_5 s$ has been computed in terms of temperature for different values of chemical potential. The curves have sharp rising by decreasing the temperature and develop finite peaks at the crossover temperature, indicating that the system degrees of freedom change rapidly during the phase transition.

References

1. R. Baier, Y.L. Dokshitzer, A.H. Mueller, S. Peigne, D. Schiff, Nucl. Phys. B **483**, 291 (1997). https://doi.org/10.1016/S0550-3213(96)00553-6. arXiv:hep-ph/9607355

2. K.J. Eskola, H. Honkanen, C.A. Salgado, U.A. Wiedemann, Nucl. Phys. A **747**, 511 (2005). https://doi.org/10.1016/j.nuclphysa.2004.09.070. arXiv:hep-ph/0406319

3. J. M. Maldacena, Int. J. Theor. Phys. **38**, 1113 (1999). https://doi.org/10.1023/A:1026654312961. https://doi.org/10.4310/ATMP.1998.v2.n2.a1. arXiv:hep-th/9711200 [Adv. Theor. Math. Phys. 2, 231 (1998)]

4. E. Witten, Adv. Theor. Math. Phys. **2**, 253 (1998). https://doi.org/10.4310/ATMP.1998.v2.n2.a2. arXiv:hep-th/9802150

5. S.S. Gubser, I.R. Klebanov, A.M. Polyakov, Phys. Lett. B **428**, 105 (1998). https://doi.org/10.1016/S0370-2693(98)00377-3. arXiv:hep-th/9802109

6. O. Aharony, S.S. Gubser, J.M. Maldacena, H. Ooguri, Y. Oz, Phys. Rep. **323**, 183 (2000). https://doi.org/10.1016/S0370-1573(99)00083-6. arXiv:hep-th/9905111

7. J. Casalderrey-Solana, H. Liu, D. Mateos, K. Rajagopal, U.A. Wiedemann, *Gauge/String Duality, Hot QCD and Heavy Ion Collisions* (Cambridge University Press, Cambridge, 2014). https://doi.org/10.1017/CBO9781139136747 arXiv:1101.0618 [hep-th]

8. J. Polchinski, M.J. Strassler. arXiv:hep-th/0003136

9. A. Karch, E. Katz, JHEP **0206**, 043 (2002). https://doi.org/10.1088/1126-6708/2002/06/043. arXiv:hep-th/0205236

10. T. Sakai, S. Sugimoto, Prog. Theor. Phys. **113**, 843 (2005). https://doi.org/10.1143/PTP.113.843. arXiv:hep-th/0412141

11. S. He, S.Y. Wu, Y. Yang, P.H. Yuan, JHEP **04**, 093 (2013). https://doi.org/10.1007/JHEP04(2013)093. arXiv:1301.0385 [hep-th]

12. Y. Yang, P.H. Yuan, JHEP **12**, 161 (2015). https://doi.org/10.1007/JHEP12(2015)161. arXiv:1506.05930 [hep-th]

13. E. Witten, Anti-de Sitter space, thermal phase transition, and confinement in gauge theories. Adv. Theor. Math. Phys. **2**, 505 (1998). arXiv:hep-th/9803131

14. J. Polchinski, M.J. Strassler, The String dual of a confining four-dimensional gauge theory. arXiv:hep-th/0003136

15. T. Sakai, S. Sugimoto, Low energy hadron physics in holographic QCD. Prog. Theor. Phys. **113**, 843 (2005). arXiv:hep-th/0412141

16. T. Sakai, S. Sugimoto, More on a holographic dual of QCD. Prog. Theor. Phys. **114**, 1083 (2005). arXiv:hep-th/0507073

17. M. Kruczenski, D. Mateos, R.C. Myers, D.J. Winters, Towards a holographic dual of large N_c QCD. JHEP **0405**, 041 (2004). arXiv:hep-th/0311270

18. A. Karch, E. Katz, Adding flavor to AdS/CFT. JHEP **0206**, 043 (2002). arXiv:hep-th/0205236

19. I.R. Klebanov, M.J. Strassler, Supergravity and a confining gauge theory: duality cascades and chi SB resolution of naked singularities. JHEP **0008**, 052 (2000). arXiv:hep-th/0007191

20. J. Erlich, E. Katz, D.T. Son, M.A. Stephanov, QCD and a holographic model of hadrons. Phys. Rev. Lett. **95**, 261602 (2005). arXiv:hep-ph/0501128

21. U. Gursoy, E. Kiritsis, Exploring improved holographic theories for QCD: Part I. JHEP **0802**, 032 (2008). arXiv:0707.1324 [hep-th]

22. U. Gursoy, E. Kiritsis, F. Nitti, Exploring improved holographic theories for QCD: Part II. JHEP **0802**, 019 (2008). arXiv:0707.1349 [hep-th]

23. U. Gursoy, E. Kiritsis, L. Mazzanti, F. Nitti, Deconfinement and gluon plasma dynamics in improved holographic QCD. Phys. Rev. Lett. **101**, 181601 (2008). arXiv:0804.0899 [hep-th]

24. U. Gursoy, E. Kiritsis, L. Mazzanti, G. Michalogiorgakis, F. Nitti, Improved holographic QCD. Lect. Notes Phys. **828**, 79 (2011). arXiv:1006.5461 [hep-th]

25. A. Buchel, Phys. Rev. D **74**, 046006 (2006). https://doi.org/10.1103/PhysRevD.74.046006. arXiv:hep-th/0605178

26. U. Gursoy, E. Kiritsis, L. Mazzanti, F. Nitti, Improved holographic Yang–Mills at finite temperature: comparison with data. Nucl. Phys. B **820**, 148 (2009). arXiv:0903.2859 [hep-th]

27. T. Alho, M. Järvinen, K. Kajantie, E. Kiritsis, K. Tuominen, On finite-temperature holographic QCD in the Veneziano limit. JHEP **1301**, 093 (2013). arXiv:1210.4516 [hep-ph]

28. T. Alho, M. Järvinen, K. Kajantie, E. Kiritsis, C. Rosen, K. Tuominen, A holographic model for QCD in the Veneziano limit at finite temperature and density. JHEP **1404**, 124 (2014). arXiv:1312.5199 [hep-ph]. Erratum: [JHEP 1502, 033 (2015)]

29. M. Järvinen, Massive holographic QCD in the Veneziano limit. JHEP **1507**, 033 (2015). arXiv:1501.07272 [hep-ph]

30. C.P. Herzog, A holographic prediction of the deconfinement temperature. Phys. Rev. Lett. **98**, 091601 (2007). arXiv:hep-th/0608151

31. A. Karch, E. Katz, D.T. Son, M.A. Stephanov, Linear confinement and AdS/QCD. Phys. Rev. D **74**, 015005 (2006). arXiv:hep-ph/0602229

32. A. Karch, E. Katz, D.T. Son, M.A. Stephanov, On the sign of the dilaton in the soft wall models. JHEP **1104**, 066 (2011). arXiv:1012.4813 [hep-ph]

33. P. Colangelo, F. Giannuzzi, S. Nicotri, V. Tangorra, Temperature and quark density effects on the chiral condensate: an AdS/QCD study. Eur. Phys. J. C **72**, 2096 (2012). arXiv:1112.4402 [hep-ph]

34. D. Dudal, D.R. Granado, T.G. Mertens, No inverse magnetic catalysis in the QCD hard and soft wall models. Phys. Rev. D **93**(12), 125004 (2016). arXiv:1511.04042 [hep-th]

35. D. Dudal, T.G. Mertens, Melting of charmonium in a magnetic field from an effective AdS/QCD model. Phys. Rev. D **91**, 086002 (2015). arXiv:1410.3297 [hep-th]

36. D. Dudal, T.G. Mertens, Radiation gauge in AdS/QCD: inadmissibility and implications on spectral functions in the deconfined phase. Phys. Lett. B **751**, 352 (2015). arXiv:1510.05490 [hep-th]

37. N. Callebaut, D. Dudal, H. Verschelde, Holographic rho mesons in an external magnetic field. JHEP **1303**, 033 (2013). arXiv:1105.2217 [hep-th]

38. T. Gherghetta, J.I. Kapusta, T.M. Kelley, Chiral symmetry breaking in the soft-wall AdS/QCD model. Phys. Rev. D **79**, 076003 (2009). arXiv:0902.1998 [hep-ph]

39. M. Panero, Thermodynamics of the QCD plasma and the large-N limit. Phys. Rev. Lett. **103**, 232001 (2009). arXiv:0907.3719 [hep-lat]

40. A. Adare et al. [PHENIX Collaboration], J/ψ production vs centrality, transverse momentum, and rapidity in Au+Au colli-

sions at $\sqrt{s_{NN}}$ = 200 GeV. Phys. Rev. Lett. **98**, 232301 (2007). arXiv:nucl-ex/0611020

41. B. B. Abelev et al. [ALICE Collaboration], Centrality, rapidity and transverse momentum dependence of J/ψ suppression in Pb-Pb collisions at $\sqrt{s_{NN}}$=2.76 TeV. Phys. Lett. B **734**, 314 (2014). arXiv:1311.0214 [nucl-ex]

42. T. Matsui, H. Satz, J/ψ suppression by quark–gluon plasma formation. Phys. Lett. B **178**, 416 (1986)

43. O. Kaczmarek, F. Zantow, Static quark anti-quark interactions in zero and finite temperature QCD. I. Heavy quark free energies, running coupling and quarkonium binding. Phys. Rev. D **71**, 114510 (2005). arXiv:hep-lat/0503017

44. K. Hashimoto, D.E. Kharzeev, Entropic destruction of heavy quarkonium in non-Abelian plasma from holography. Phys. Rev. D **90**(12), 125012 (2014). arXiv:1411.0618 [hep-th]

45. J.M. Maldacena, Phys. Rev. Lett. **80**, 4859 (1998). https://doi.org/10.1103/PhysRevLett.80.4859. arXiv:hep-th/9803002

46. S.J. Rey, J.T. Yee, Eur. Phys. J. C **22**, 379 (2001). https://doi.org/10.1007/s100520100799. arXiv:hep-th/9803001

47. S.J. Rey, S. Theisen, J.T. Yee, Nucl. Phys. B **527**, 171 (1998). https://doi.org/10.1016/S0550-3213(98)00471-4. arXiv:hep-th/9803135

48. I. Iatrakis, D.E. Kharzeev, Holographic entropy and real-time dynamics of quarkonium dissociation in non-Abelian plasma. Phys. Rev. D **93**(8), 086009 (2016). arXiv:1509.08286 [hep-ph]

49. K. Bitaghsir Fadafan, S.K. Tabatabaei, Entropic destruction of a moving heavy quarkonium. Phys. Rev. D **94**(2), 026007 (2016). arXiv:1512.08254 [hep-ph]

50. Z.Q. Zhang, C. Ma, D.F. Hou, G. Chen, Entropic destruction of a rotating heavy quarkonium. arXiv:1611.08011 [hep-th]

51. D. Dudal, S. Mahapatra, JHEP **1807**, 120 (2018). https://doi.org/10.1007/JHEP07(2018)120. arXiv:1805.02938 [hep-th]

52. D. Dudal, S. Mahapatra, Phys. Rev. D **96**(12), 126010 (2017). https://doi.org/10.1103/PhysRevD.96.126010. arXiv:1708.06995 [hep-th]

53. H. Bohra, D. Dudal, A. Hajilou, S. Mahapatra, Phys. Lett. B **801**, 135184 (2020). https://doi.org/10.1016/j.physletb.2019.135184. arXiv:1907.01852 [hep-th]

54. S.S. Jena, B. Shukla, D. Dudal, S. Mahapatra, Phys. Rev. D **105**(8), 086011 (2022). https://doi.org/10.1103/PhysRevD.105.086011. arXiv:2202.01486 [hep-th]

55. R. Sommer, Nucl. Phys. B **411**, 839–854 (1994). https://doi.org/10.1016/0550-3213(94)90473-1. arXiv:hep-lat/9310022 [hep-lat]

56. J. Adams et al. [STAR Collaboration], Nucl. Phys. A **757**, 102 (2005). https://doi.org/10.1016/j.nuclphysa.2005.03.085. arXiv:nucl-ex/0501009

57. K. Adcox et al. [PHENIX Collaboration], Nucl. Phys. A **757**, 184 (2005). https://doi.org/10.1016/j.nuclphysa.2005.03.086. arXiv:nucl-ex/0410003

58. I. Arsene et al. [BRAHMS Collaboration], Nucl. Phys. A **757**, 1 (2005). https://doi.org/10.1016/j.nuclphysa.2005.02.130. arXiv:nucl-ex/0410020

59. B.B. Back et al., Nucl. Phys. A **757**, 28 (2005). https://doi.org/10.1016/j.nuclphysa.2005.03.084. arXiv:nucl-ex/0410022

60. Z.B. Yin [ALICE Collaboration], Acta Phys. Polon. Supp. **6**, 479 (2013). https://doi.org/10.5506/APhysPolBSupp.6.479

61. G. Aad et al. [ATLAS Collaboration], Phys. Rev. Lett. **105**, 252303 (2010). https://doi.org/10.1103/PhysRevLett.105.252303. arXiv:1011.6182 [hep-ex]

62. S. Chatrchyan et al. [CMS Collaboration], Phys. Rev. C **84**, 024906 (2011). https://doi.org/10.1103/PhysRevC.84.024906. arXiv:1102.1957 [nucl-ex]

63. K.M. Burke et al. [JET Collaboration], Phys. Rev. C **90**(1), 014909 (2014). https://doi.org/10.1103/PhysRevC.90.014909. arXiv:1312.5003 [nucl-th]

64. F. D'Eramo, H. Liu, K. Rajagopal, Phys. Rev. D **84**, 065015 (2011). https://doi.org/10.1103/PhysRevD.84.065015. arXiv:1006.1367 [hep-ph]

65. R. Rapp, H. van Hees. https://doi.org/10.1142/9789814293297_0003. arXiv:0903.1096 [hep-ph]

66. J. Dunkel, P. Hänggi, Phys. Rep. **471**, 1–73 (2009). https://doi.org/10.1016/j.physrep.2008.12.001. arXiv:0812.1996 [cond-mat.stat-mech]

67. T. Domurcukgul, R. Morad, Eur. Phys. J. C **82**(4), 304 (2022). https://doi.org/10.1140/epjc/s10052-022-10252-w. arXiv:2108.10853 [hep-th]

68. A.K. Mes, R.W. Moerman, J.P. Shock, W.A. Horowitz, Ann. Phys. **436**, 168675 (2022). https://doi.org/10.1016/j.aop.2021.168675. arXiv:2008.09196 [hep-th]

69. E. Caceres, A. Guijosa, JHEP **11**, 077 (2006). https://doi.org/10.1088/1126-6708/2006/11/077. arXiv:hep-th/0605235 [hep-th]

70. S. Chakraborty, N. Haque, JHEP **12**, 175 (2014). https://doi.org/10.1007/JHEP12(2014)175. arXiv:1410.7040 [hep-th]

71. L. Cheng, X.H. Ge, S.Y. Wu, Eur. Phys. J. C **76**(5), 256 (2016). https://doi.org/10.1140/epjc/s10052-016-4096-7. arXiv:1412.8433 [hep-th]

72. K.B. Fadafan, JHEP **12**, 051 (2008). https://doi.org/10.1088/1126-6708/2008/12/051. arXiv:0803.2777 [hep-th]

73. T. Matsuo, D. Tomino, W.Y. Wen, JHEP **10**, 055 (2006). https://doi.org/10.1088/1126-6708/2006/10/055. arXiv:hep-th/0607178

74. P. Talavera, JHEP **01**, 086 (2007). https://doi.org/10.1088/1126-6708/2007/01/086. arXiv:hep-th/0610179

75. Z.Q. Zhang, K. Ma, D.F. Hou, J. Phys. G **45**(2), 025003 (2018). https://doi.org/10.1088/1361-6471/aaa097. arXiv:1802.01912 [hep-th]

76. O. Andreev, Phys. Rev. D **98**(6), 066007 (2018). https://doi.org/10.1103/PhysRevD.98.066007. arXiv:1804.09529 [hep-ph]

77. J. Sadeghi, M.R. Setare, B. Pourhassan, S. Hashmatian, Eur. Phys. J. C **61**, 527–533 (2009). https://doi.org/10.1140/epjc/s10052-009-1011-5. arXiv:0901.0217 [hep-th]

78. S.S. Gubser, Phys. Rev. D **76**, 126003 (2007). https://doi.org/10.1103/PhysRevD.76.126003. arXiv:hep-th/0611272

79. C.P. Herzog, A. Karch, P. Kovtun, C. Kozcaz, L.G. Yaffe, JHEP **07**, 013 (2006). https://doi.org/10.1088/1126-6708/2006/07/013. arXiv:hep-th/0605158

80. M. Chernicoff, D. Fernandez, D. Mateos, D. Trancanelli, JHEP **08**, 100 (2012). https://doi.org/10.1007/JHEP08(2012)100. arXiv:1202.3696 [hep-th]

81. A. Nata Atmaja, K. Schalm, JHEP **04**, 070 (2011). https://doi.org/10.1007/JHEP04(2011)070. arXiv:1012.3800 [hep-th]

82. K.L. Panigrahi, S. Roy, JHEP **04**, 003 (2010). https://doi.org/10.1007/JHEP04(2010)003. arXiv:1001.2904 [hep-th]

83. Y. Xiong, X. Tang, Z. Luo, Chin. Phys. C **43**(11), 113103 (2019). https://doi.org/10.1088/1674-1137/43/11/113103. arXiv:1909.00928 [hep-ph]

84. U. Gursoy, E. Kiritsis, G. Michalogiorgakis, F. Nitti, JHEP **12**, 056 (2009). https://doi.org/10.1088/1126-6708/2009/12/056. arXiv:0906.1890 [hep-ph]

85. S.S. Gubser, Phys. Rev. D **74**, 126005 (2006). https://doi.org/10.1103/PhysRevD.74.126005. arXiv:hep-th/0605182

86. D. Giataganas, H. Soltanpanahi, JHEP **06**, 047 (2014). https://doi.org/10.1007/JHEP06(2014)047. arXiv:1312.7474 [hep-th]

87. Z.R. Zhu, J.X. Chen, X.M. Liu, D. Hou, Eur. Phys. J. C **82**(6), 560 (2022). https://doi.org/10.1140/epjc/s10052-022-10433-7. arXiv:2109.02366 [hep-ph]

88. S.S. Gubser, Nucl. Phys. B **790**, 175–199 (2008). https://doi.org/10.1016/j.nuclphysb.2007.09.017. arXiv:hep-th/0612143

89. J. Casalderrey-Solana, D. Teaney, Phys. Rev. D **74**, 085012 (2006). https://doi.org/10.1103/PhysRevD.74.085012. arXiv:hep-ph/0605199

90. J. Casalderrey-Solana, D. Teaney, JHEP **04**, 039 (2007). https://doi.org/10.1088/1126-6708/2007/04/039. arXiv:hep-th/0701123

91. J. de Boer, V.E. Hubeny, M. Rangamani, M. Shigemori, JHEP **07**, 094 (2009). https://doi.org/10.1088/1126-6708/2009/07/094. arXiv:0812.5112 [hep-th]

92. D.T. Son, D. Teaney, JHEP **07**, 021 (2009). https://doi.org/10.1088/1126-6708/2009/07/021. arXiv:0901.2338 [hep-th]

93. G.C. Giecold, E. Iancu, A.H. Mueller, JHEP **07**, 033 (2009). https://doi.org/10.1088/1126-6708/2009/07/033. arXiv:0903.1840 [hep-th]

94. N. Iqbal, H. Liu, Phys. Rev. D **79**, 025023 (2009). https://doi.org/10.1103/PhysRevD.79.025023. arXiv:0809.3808 [hep-th]

95. U. Gursoy, E. Kiritsis, L. Mazzanti, F. Nitti, JHEP **12**, 088 (2010). https://doi.org/10.1007/JHEP12(2010)088. arXiv:1006.3261 [hep-th]

96. D. Giataganas, H. Soltanpanahi, Phys. Rev. D **89**(2), 026011 (2014). https://doi.org/10.1103/PhysRevD.89.026011. arXiv:1310.6725 [hep-th]

97. E. Kiritsis, L. Mazzanti, F. Nitti, JHEP **02**, 081 (2014). https://doi.org/10.1007/JHEP02(2014)081. arXiv:1311.2611 [hep-th]

98. V. Mykhaylova, C. Sasaki, Phys. Rev. D **103**(1), 014007 (2021). https://doi.org/10.1103/PhysRevD.103.014007. arXiv:2007.06846 [hep-ph]

99. X. Zhu, Z.Q. Zhang, Eur. Phys. J. A **57**(3), 96 (2021). https://doi.org/10.1140/epja/s10050-021-00418-7. arXiv:2011.00920 [nucl-th]

100. H. Liu, K. Rajagopal, U.A. Wiedemann, Phys. Rev. Lett. **97**, 182301 (2006). https://doi.org/10.1103/PhysRevLett.97.182301. arXiv:hep-ph/0605178

101. R. Rougemont, A. Ficnar, S. Finazzo, J. Noronha, JHEP **1604**, 102 (2016). https://doi.org/10.1007/JHEP04(2016)102. arXiv:1507.06556 [hep-th]

102. D. Li, J. Liao, M. Huang, Phys. Rev. D **89**(12), 126006 (2014). https://doi.org/10.1103/PhysRevD.89.126006. arXiv:1401.2035 [hep-ph]

103. A. Brandhuber, N. Itzhaki, J. Sonnenschein, S. Yankielowicz, Phys. Lett. B **434**, 36 (1998). https://doi.org/10.1016/S0370-2693(98)00730-8. arXiv:hep-th/9803137

104. J. Sonnenschein. arXiv:hep-th/0003032

105. H. Liu, K. Rajagopal, U.A. Wiedemann, JHEP **0703**, 066 (2007). https://doi.org/10.1088/1126-6708/2007/03/066. arXiv:hep-ph/0612168

106. E. Caceres, A. Guijosa, JHEP **0612**, 068 (2006). https://doi.org/10.1088/1126-6708/2006/12/068. arXiv:hep-th/0606134

107. J.F. Vazquez-Poritz. arXiv:hep-th/0605296

108. E. Nakano, S. Teraguchi, W.Y. Wen, Phys. Rev. D **75**, 085016 (2007). https://doi.org/10.1103/PhysRevD.75.085016. arXiv:hep-ph/0608274

109. S.D. Avramis, K. Sfetsos, JHEP **0701**, 065 (2007). https://doi.org/10.1088/1126-6708/2007/01/065. arXiv:hep-th/0606190

110. Y.H. Gao, W.S. Xu, D.F. Zeng. arXiv:hep-th/0611217

111. N. Armesto, J.D. Edelstein, J. Mas, JHEP **0609**, 039 (2006). https://doi.org/10.1088/1126-6708/2006/09/039. arXiv:hep-ph/0606245

112. F.L. Lin, T. Matsuo, Phys. Lett. B **641**, 45 (2006). https://doi.org/10.1016/j.physletb.2006.08.024. arXiv:hep-th/0606136

113. J. Sadeghi, S. Heshmatian, Eur. Phys. J. C **74**, 3032 (2014). https://doi.org/10.1140/epjc/s10052-014-3032-y. arXiv:1308.5991 [hep-th]

114. R.G. Cai, S. Chakrabortty, S. He, L. Li, JHEP **1302**, 068 (2013). https://doi.org/10.1007/JHEP02(2013)068. arXiv:1209.4512 [hep-th]

115. L. Wang, S.Y. Wu, Eur. Phys. J. C **76**(11), 587 (2016). https://doi.org/10.1140/epjc/s10052-016-4421-1. arXiv:1609.03665 [hep-th]

116. O. DeWolfe, C. Rosen, JHEP **0907**, 022 (2009). https://doi.org/10.1088/1126-6708/2009/07/022. arXiv:0903.1458 [hep-th]

117. K. Bitaghsir Fadafan, Eur. Phys. J. C **68**, 505 (2010). https://doi.org/10.1140/epjc/s10052-010-1375-6. arXiv:0809.1336 [hep-th]

118. W.A. Horowitz, Nucl. Part. Phys. Proc. **289–290**, 129 (2017). https://doi.org/10.1016/j.nuclphysbps.2017.05.026

119. W.A. Horowitz, Phys. Rev. D **91**(8), 085019 (2015). https://doi.org/10.1103/PhysRevD.91.085019. arXiv:1501.04693 [hep-ph]

120. S. Heshmatian, R. Morad, M. Akbari, JHEP **03**, 045 (2019). https://doi.org/10.1007/JHEP03(2019)045. arXiv:1812.09374 [hep-th]

121. D. Giataganas, JHEP **07**, 031 (2012). https://doi.org/10.1007/JHEP07(2012)031. arXiv:1202.4436 [hep-th]

122. R. Morad, W.A. Horowitz, JHEP **1411**, 017 (2014). https://doi.org/10.1007/JHEP11(2014)017. arXiv:1409.7545 [hep-th]

123. K. Bitaghsir Fadafan, R. Morad, Eur. Phys. J. C **78**(1), 16 (2018). https://doi.org/10.1140/epjc/s10052-018-5520-y. arXiv:1710.06417 [hep-th]

124. P.M. Chesler, K. Jensen, A. Karch, L.G. Yaffe, Phys. Rev. D **79**, 125015 (2009). https://doi.org/10.1103/PhysRevD.79.125015. arXiv:0810.1985 [hep-th]

125. A. Ficnar, J. Noronha, M. Gyulassy, J. Phys. G **38**, 124176 (2011). https://doi.org/10.1088/0954-3899/38/12/124176. arXiv:1106.6303 [hep-ph]

126. P.M. Chesler, K. Jensen, A. Karch, Phys. Rev. D **79**, 025021 (2009). https://doi.org/10.1103/PhysRevD.79.025021. arXiv:0804.3110 [hep-th]

127. B.G. Zakharov, JETP Lett. **65**, 615 (1997). https://doi.org/10.1134/1.567389. arXiv:hep-ph/9704255

128. Q. Zhou, B.W. Zhang, Commun. Theor. Phys. **75**(10), 105301 (2023). https://doi.org/10.1088/1572-9494/acea23. arXiv:2211.14792 [hep-ph]

129. I.Y. Aref'eva, K. Rannu, P. Slepov, JHEP **06**, 090 (2021). https://doi.org/10.1007/JHEP06(2021)090. arXiv:2009.05562 [hep-th]